

# Theoretical model of hydrodynamic jet formation from accretion disks with turbulent viscosity

E. Arshilava<sup>a,b</sup>, M. Gogilashvili<sup>a,c</sup>, V. Loladze<sup>a,c</sup>, I. Jokhadze<sup>a</sup>, B. Modrekiladze<sup>a,d</sup>, N. L. Shatashvili<sup>a,e</sup>, A. G. Tevzadze<sup>a,d,f</sup>

<sup>a</sup>Department of Physics, Faculty of Exact and Natural Sciences, Javakishvili Tbilisi State University (TSU), Tbilisi 0179, Georgia

<sup>b</sup>Department of Physics and Astronomy, Heidelberg University, 69120, Heidelberg, Germany

<sup>c</sup>Department of Physics, Florida State University, Tallahassee, FL 32306, USA

<sup>d</sup>Department of Physics, Carnegie Mellon University, 5000 Forbes Ave., Pittsburgh, PA 15213, USA

<sup>e</sup>TSU Andronikashvili Institute of Physics, TSU, Tbilisi 0177, Georgia

<sup>f</sup>Abastumani Astrophysical Observatory, Ilia State University, 3/5 Cholokashvili Ave., Tbilisi 0162, Georgia

## Abstract

We develop the theoretical model for the analytic description of hydrodynamic jets from protostellar disks employing the Beltrami-Bernoulli flow configuration of disk-jet structure. For this purpose we extend the standard turbulent viscosity prescription and derive several classes of analytic solutions using the flow parametrization in self-similar variables. Derived solutions describe the disk-jet structure, where for the first time jet properties are analytically linked with the properties of the accretion disk flow. The ratio of the jet ejection and disk accretion velocities is controlled by the turbulence parameter, while the ejection velocity increases with the decrease of local sound velocity and the jet launching radius. Derived solutions can be used to analyze the astrophysical jets from protostellar accretion disks and link the properties of outflows with the local observational properties of accretion disk flows.

*Keywords:*

Accretion, accretion discs, Galaxies: jets, Galaxies: structure

## 1. Introduction

Jets streaming from young stellar objects (YSOs) are spectacular manifestations of the star formation process. These outflows, believed to be powered by protostellar accretion disk, carry away the matter, energy and angular momentum of the accreting matter, thus promoting the development of a protostar. Properties of these disk-jet systems are inferred from the observations of Herbig-Haro (HH) objects, T-Tauri and Herbig Ae/Be stars, protostellar and protoplanetary disks.

Collimated bipolar outflows from YSO are known to be parsec-scale, non-relativistic and supersonic by nature. The radial velocity of the jet-flow varies from 20 km/s up to 450 km/s for HH jets (see Hartigan et al. 2011; Plunkett et al. 2015; Podio et al. 2016; Jhan & Lee 2016; Bjerkeli et al. 2016; Reiter et al. 2017). These jets are launched in the vicinity of a protostar, as close as 0.03au (see Lee et al. 2017). A vast number of collimated jets are detected in molecular clouds pointing to the embedded protostars. Surveys of these jets (see, e.g., Ioannidis & Froebrich 2012; Smith et al. 2014; Zhang et al. 2014) provide a large unbiased observational data that can be used to test the theoretical models of the disk-jet structures. Today we know that morphology, sizes and velocities of the jet-outflows can be used to estimate the mass, luminosity and/or age of the YSOs (see Bally 2016 and references therein).

Another class of wide-angle hydrodynamic outflows from HH objects decelerate either with increasing the angle away from the central axis of the flow, or increasing distance along

axis (see Lizano 1988). It is known that these hydrodynamic outflows of neutral atoms are intrinsically linked with the process of star formation (see, e.g., Ruden et al. 1990, Shu et al. 1991).

The main mass/energy source of the ejecta is the disk-flow material/energy released through the accretion process. Hence, jet velocities are intrinsically correlated with the accretion rates calling for the unified treatment of the disk-jet system dynamics. The central object dynamics may play the additional role in the formation of relativistic outflows/jets [Livio 1997– powerful jets are produced by systems in which on top of an accretion disk threaded by a vertical field, there exists an additional source of energy/wind, possibly associated with the central object (for example, stellar wind from protostar may accelerate YSO jets, as estimated by Ferreira 1996; Ferreira et al. 2006,2007)]. In (Shatashvili & Yoshida 2011) it was shown, that there exists a general principle that dictates a marked similarity in macroscopic disk-jet geometry despite the huge variety of the scaling parameters such as Lorentz factor, Reynolds number, Lundquist number, ionization fractions, etc., characterizing different systems.

A class of the hydrodynamic jet solution from viscous accretion flows has been studied by Scott & Lovelace 1987. Self-similar solutions of the model give velocity field being inverse proportional to the radial distance from the center. Matching the profiles of circular jets (Squire 1951) this solution deviates from the Keplerian profile and can be effectively used outside the accretion disk area. Another solution to the formation of

hydrodynamic jets has been studied by Hernandez et al. 2014 showing that under certain conditions hydrodynamic accretion disk can develop instabilities. Using perturbation analysis authors have shown that developed instability may lead to the formation of pair of bipolar jet-outflows. Instability mechanism is unlikely to support a steady disk-jet structure, and can possibly be used in the description of short time outbursts from the hydrodynamic accretion flows in the vicinity of central object. Recently Clarke & Alexander 2016 have used a self-similar approach for the description of the axisymmetric hydrodynamic outflows from hydrodynamic accretion disks. Authors have shown isothermal disk-wind structure that can be developed for the power low density profile that well matches the results of numerical simulations in the wind area.

Since the viscous accretion disk model was proposed (Shakura & Sunyaev 1973), with an observed high ejection efficiency, it became natural to assume that jets are driven magnetically from an accretion disk — when magnetic field is advected inwards by accreting material or/and generated locally by some mechanism, the centrifugal force due to rotation may boost the jet along the magnetic field lines up to a super-Alfvénic speed, (Begelman et al. 1984; Begelman 1993, 1998; Celotti & Blandford 2001; Kudoh & Shibata 1997; Kuwabara et al. 2005; Anderson et al. 2005). Blandford & Payne (1982) studied the magneto-centrifugal acceleration along the magnetic field lines and demonstrated that the magnetic field results into instability of particles at the Kepler orbit leading to the Jet formation in the disk center (with the opening angle of the jet  $\leq 30^\circ$ ). They were the first to show the braking of matter in the azimuthal direction inside the disk and the outflow acceleration above the disk surface guided by the poloidal magnetic field components. Toroidal components of the magnetic field then collimate the flow. In the case of the fully turbulent Keplerian disk the poloidal magnetic field tends to drift outward (Lovelace et al. 1994; Lubow et al. 1994; Bisnovatyi-Kogan & Lovelace 2007) so that its value cannot significantly exceed the strength of the large-scale seed magnetic field. Then, according to the hydro-magnetic models, the magnetic fields provide a natural mechanical link between disks and jets and can account for the launching, confinement and collimation of jets (see e.g. (Blandford & Rees 1974; Blandford & Znajek 1997; Blandford & Payne 1982; Blandford 1994; Krasnopolsky et al. 1999; Zanni et al. 2007)) — the angular momentum, energy and mass can be removed from the accreting flow. The collimation is provided by the stratified thermal pressure from an external medium while the acceleration efficiency then depends on the pressure gradient of the medium.

In the present paper we present the results of theoretical study of the disk-jet structure formation for YSOs based on the Beltrami Flow model (Shatashvili & Yoshida 2011) using the Turbulent Viscosity approach (Shakura & Sunyaev 1973) as the main reason of accretion; disk was assumed un-magnetized, hence, there is no pre-existed global magnetic field. We have found the analytical conditions for disk-jet structure formation and parameter ranges for Jet-launching and collimation for YSO Jets.

The Physical model of the problem is described in Sec 2

where we derive the extended turbulent viscosity model and use it in the model equations for the disk-jet flows. Using the similarity variables and variable splitting ansatz we derive several classes of the solutions, which includes the flow configuration of the accretion disk–ejection jet structure. We use specific examples to illustrate the disk-jet structures and explore their properties. The paper is summarized in Sec. 3.

## 2. Physical Model

YSO disk-jet structure, according to observations, is quite a long-lived object. Hence, the steady state solutions could well describe its behavior. Equations governing the dynamics of the stationary viscous compressible fluid rotating around a central gravitating object can be written as follows:

$$(\mathbf{V} \cdot \nabla)\mathbf{V} = -\nabla H - \nabla\Phi + \frac{1}{\rho}\nabla \cdot \mathbf{T}, \quad (1)$$

$$\nabla \cdot (\rho\mathbf{V}) = 0, \quad (2)$$

where  $\mathbf{V}$ ,  $\rho$  and  $H$  are the velocity, density and enthalpy, respectively;  $\Phi$  is the gravitational potential of the central object; it is assumed, that the gravity of disk can be ignored. Dissipative effects are described by the viscous stress tensor  $T_{ik}$  and the corresponding term in Eq.(1) is formally written as:

$$\nabla \cdot \mathbf{T} \equiv \nabla_k T_{ik} = \frac{\partial}{\partial x_k} T_{ik}. \quad (3)$$

The barotropic equation of state (for our problem of study) was used to calculate the enthalpy of the fluid:

$$\nabla H = \frac{1}{\rho}\nabla\mathcal{P}, \quad (4)$$

where  $\mathcal{P}$  is the thermodynamic pressure. To seek for the steady state solutions of the disc-jet structures persisting around a central accreting object we introduce a so-called “ideal” and “reduced” factors of the “local” density following Shatashvili & Yoshida (2011); Yoshida & Shatashvili (2012):

$$\rho = \rho_I \rho_R. \quad (5)$$

The purpose of this separation is to separate ideal fluid and dissipative effects and to track the accretion effects in jet formation process. Thus, in conventional ideal fluid mechanics with zero dissipation  $\rho_R = 1$  and  $\rho_I = \rho$ . In such formalism we can introduce “ideal” and “reduced” momenta as:

$$\mathbf{P}_I = \rho_I \mathbf{V}, \quad (6)$$

$$\mathbf{P}_R = \rho_R \mathbf{V}. \quad (7)$$

Obviously, the reduced momentum matches flow velocity in fluids with zero dissipation. Reformulating Eqs. (1,2) in terms of the new momenta we can derive a “Generalized Pressure Balance equation” in our definitions as follows:

$$\mathbf{P}_R \times (\nabla \times \mathbf{P}_R) = \quad (8)$$

$$= \frac{1}{2} \nabla P_R^2 + \rho_R^2 \nabla (H + \Phi) + \frac{\rho_R}{\rho_I} [\mathbf{P}_R (\nabla \cdot \mathbf{P}_I) + \nabla \cdot \mathbf{T}].$$

We will later use this equation to define the topology of the fluid and reduced components of the disk-jet system. Firstly, the geometry of the problem allows the assumption for the reduced momentum to obey the Beltrami Condition implying that the Reduced Momentum is aligning along its corresponding Generalized Vorticity (see e.g. Shatashvili & Yoshida 2011; Yoshida & Shatashvili 2012 and references therein):

$$\mathbf{P}_R = \lambda (\nabla \times \mathbf{P}_R), \quad (9)$$

thus making the left hand side term strictly zero in the Eq. (8). Here  $\lambda$  stands for the Beltrami parameter related to the so called flow reduced momentum. Secondly, we seek for the solution of the fluid reduced momentum that will make the last term zero on the r.h.s. of the Eq. (8), thus, fully determined by the viscosity effect:

$$\mathbf{P}_R (\nabla \cdot \mathbf{P}_I) + \nabla \cdot \mathbf{T} = 0. \quad (10)$$

Using such assumptions pressure balance equation (8) reduces to a ‘‘Generalized Bernoulli Condition’’ written for the reduced momentum and the reduced density of the flow:

$$\frac{1}{2} \nabla P_R^2 + \rho_R^2 \nabla (H + \Phi) = 0. \quad (11)$$

Hence, the stationary state of the system can be fully analyzed using Eqs. (9,10,11) and the explicit form of the viscous stress tensor related to the specific YSO conditions. Note that the Eqs. (10) and (11) are valid only in the case of dissipative flow ( $\mathbf{T} \neq 0$ ), while inviscid Beltrami flow ( $\mathbf{T} = 0$ ) can be described by the Eq. (8) with the corresponding right hand side.

### 2.1. Turbulent viscosity model

The radial outward momentum transfer and consequent inward accretion is due to the dissipative processes induced by the turbulence in the disk-jet flow. Hence, we employ the turbulent viscosity model when the small scale turbulence creates the anomalous dissipation that can be described by using the  $\alpha$ -viscosity model introduced by Shakura & Sunyaev (1973). In contrast to the standard  $\alpha$  model, we plan to use the effective viscosity model both in the disk and jet as well as in the disk-jet transition areas.

We employ cylindrical coordinates  $(r, \varphi, z)$  to describe the disk-jet system. Hence, the only significant components of the viscous stress tensor  $T_{ik}$ , assuming the strong azimuthal rotation, will be:

$$T_{r\varphi} = T_{\varphi r} = \nu_t \rho \left[ r \frac{\partial}{\partial r} \left( \frac{V_\varphi}{r} \right) + \frac{1}{r} \frac{\partial V_r}{\partial \varphi} \right], \quad (12)$$

$$T_{z\varphi} = T_{\varphi z} = \nu_t \rho \left[ \frac{\partial V_\varphi}{\partial z} + \frac{1}{r} \frac{\partial V_z}{\partial \varphi} \right], \quad (13)$$

where  $\nu_t$  is the turbulent viscosity parameter. We now split the pressure  $\mathcal{P}$  into the background constant component  $\mathcal{P}_0$  and  $p$  being a deviation from this background value:

$$\mathcal{P} = \mathcal{P}_0 + p. \quad (14)$$

In this limit the turbulent stress tensor can be split into the background constant component  $\bar{T}_{ik}$  and smaller deviation  $t_{ik}$  that varies with spatial coordinate:

$$T_{ik} = \bar{T}_{ik} + t_{ik}. \quad (15)$$

The classical  $\alpha$ -viscosity model links turbulent viscosity stress tensor to the pressure using the constant parameter  $\alpha_0$ :

$$\bar{T}_{r\varphi} = \alpha_0 \mathcal{P}_0. \quad (16)$$

Assuming axisymmetric flow  $V_\varphi = r \Omega_K(r, z)$  rotating locally with Keplerian angular velocity:

$$\Omega_K^2(r, z) = \frac{GM_\star}{(r^2 + z^2)^{3/2}}, \quad (17)$$

where  $M_\star$  is the mass of the central object, we can extend the standard turbulent viscosity model to derive:

$$t_{ik} \equiv \left\langle \frac{3}{2} \nu_t \rho \Omega_K(r, z) \right\rangle \frac{r^2}{r^2 + z^2} - \alpha_0 \mathcal{P}_0. \quad (18)$$

Hence, in the axisymmetric case, when the azimuthal gradients in the Eqs. (12,13) can be neglected, the viscous stress tensor elements can be calculated as follows:

$$t_{r\varphi} = \frac{r^2}{r^2 + z^2} \beta p, \quad (19)$$

$$t_{z\varphi} = \frac{rz}{r^2 + z^2} \beta p. \quad (20)$$

Here  $p$  can be positive/negative, corresponding to the stronger/weaker turbulence compared to the background turbulent steady state. Assumption of the strictly Keplerian local angular velocity of the rotation (see Eq. (17)) can be justified for the rotationally supported flow, for which the radial pressure gradients can be negligible compared to the centrifugal force. Such situation is realized in slowly accreting flows, where background pressure is known to vary slowly, i.e.,  $\mathcal{P}_0 = \text{const.}$ ).

### 2.2. Model Equations for Disk-Jet Structure

Dictated by the geometry of observed YSOs disk-jet structure and the continuity Eq. (2), let us expand the flow velocity using the axisymmetric stream function  $\psi$  and local Keplerian azimuthal circulation, as follows:

$$\mathbf{V} = \frac{1}{\rho} (\nabla \psi \times \nabla \varphi) + r V_\varphi \nabla \varphi. \quad (21)$$

Interestingly, the  $\psi$  introduced in such a way matches the stream function of the actual momentum  $\mathbf{P} = \rho \mathbf{V}$  of the flow. Now we can reformulate our problem in terms of the stream function  $\psi$  using the turbulent viscosity stress tensor calculated in the previous subsection. Hence, Eq. (10) takes the following form:

$$\frac{V_\varphi}{r} \left( \frac{\partial \psi}{\partial r} \frac{\partial}{\partial z} \ln \rho_R - \frac{\partial \psi}{\partial z} \frac{\partial}{\partial r} \ln \rho_R \right) = \beta \frac{r^2}{r^2 + z^2} \left[ \frac{\partial p}{\partial r} + \frac{z}{r} \frac{\partial p}{\partial z} + \frac{2\beta}{r} p \right], \quad (22)$$

while the generalized Bernoulli Condition (11) will be reduced to the following:

$$\nabla \mathcal{E}_m + \left( V_\varphi^2 + \frac{(\nabla \psi)^2}{r^2 \rho^2} \right) \nabla \ln \rho_R = 0, \quad (23)$$

where we have introduced the total mechanical energy  $\mathcal{E}_m$  as follows:

$$\mathcal{E}_m \equiv \Phi + \frac{V_\varphi^2}{2} + \frac{(\nabla \psi)^2}{2r^2 \rho^2}. \quad (24)$$

The system of equations describing the YSOs disk-jet structure can be closed using the Beltrami condition (9) written in the stream function representation:

$$\nabla \times \nabla \psi \times \nabla \varphi + \nabla \times [(\rho r V_\varphi) \nabla \varphi] + \nabla \psi \times \nabla \varphi \times \nabla \ln \rho_I + (\rho r V_\varphi) \nabla \varphi \times \nabla \ln \rho_I = \lambda (\nabla \psi \times \nabla \varphi + (\rho r V_\varphi) \nabla \varphi). \quad (25)$$

Hence, the system is reduced to the Eqs. (22,23,24) and (25).

### 2.3. Equations in the similarity variables

To construct the similarity solution of the system of equations (22-25) representing disk-jet structure we introduce the orthogonal variables  $\tau$  and  $\sigma$  as follows:

$$\sigma = \sqrt{r^2 + z^2}, \quad (26)$$

$$\tau = z/r, \quad (27)$$

for which  $\nabla \tau \cdot \nabla \sigma = 0$ . Then, the derivatives in  $r$  and  $z$  variables can be expressed as:

$$\begin{aligned} \frac{\partial}{\partial r} &= -\frac{z}{r^2} \frac{\partial}{\partial \tau} + \frac{r}{\sqrt{r^2 + z^2}} \frac{\partial}{\partial \sigma} \\ &= -\frac{\tau \sqrt{1 + \tau^2}}{\sigma} \frac{\partial}{\partial \tau} + \frac{1}{\sqrt{1 + \tau^2}} \frac{\partial}{\partial \sigma}, \end{aligned} \quad (28)$$

$$\begin{aligned} \frac{\partial}{\partial z} &= \frac{1}{r} \frac{\partial}{\partial \tau} + \frac{z}{\sqrt{r^2 + z^2}} \frac{\partial}{\partial \sigma} \\ &= \frac{\sqrt{1 + \tau^2}}{\sigma} \frac{\partial}{\partial \tau} + \frac{\tau}{\sqrt{1 + \tau^2}} \frac{\partial}{\partial \sigma}. \end{aligned} \quad (29)$$

The first obvious result of such coordinates is that the Gravitational Potential depends only on one variable:  $\Phi = \Phi(\sigma) = -\Omega_0^2/\sigma$ . While the natural representation of velocity given by (21) allows the simplifying assumption for the stream function to be dependent only on the  $\tau$  variable:

$$\psi = \psi(\tau), \quad (30)$$

thus, making it possible to separate the variables in the solution. Then, the Eq. (22) will take the following form in the similarity variables:

$$V_\varphi \frac{1 + \tau^2}{\sigma^2} \frac{\partial \psi}{\partial \tau} \frac{\partial}{\partial \sigma} \ln \rho_R = \left( \frac{\partial}{\partial \sigma} + \frac{2}{\sigma} \right) \frac{\beta p}{1 + \tau^2}, \quad (31)$$

The three components  $r, \varphi, z$  of the Beltrami conditions (25) in the new variables yield the following three equations, respectively:

$$\left( \frac{\tau \sigma^2}{(1 + \tau^2)^{3/2}} \frac{\partial}{\partial \sigma} + \frac{\partial}{\partial \tau} \right) \ln \left( \frac{\sigma \rho_R V_\varphi}{(1 + \tau^2)^{1/2}} \right) = \frac{\lambda}{\rho V_\varphi} \frac{\partial \psi}{\partial \tau}, \quad (32)$$

$$\frac{\partial^2 \psi}{\partial \tau^2} + \left( \frac{3\tau}{1 + \tau^2} - \frac{\partial}{\partial \tau} \ln \rho_I \right) \frac{\partial \psi}{\partial \tau} = -\lambda \frac{\sigma^3}{(1 + \tau^2)^{5/2}} \rho V_\varphi, \quad (33)$$

$$\left( -\frac{\sigma^2}{\tau(1 + \tau^2)^{3/2}} \frac{\partial}{\partial \sigma} + \frac{\partial}{\partial \tau} \right) \ln \left( \frac{\sigma \rho_R V_\varphi}{(1 + \tau^2)^{1/2}} \right) = \frac{\lambda}{\rho V_\varphi} \frac{\partial \psi}{\partial \tau}. \quad (34)$$

Equations (32) and (34), after some straightforward algebra, lead to following elegant equations:

$$\frac{\partial}{\partial \sigma} \left( \frac{\sigma}{(1 + \tau^2)^{1/2}} \rho V_\varphi \right) = 0, \quad (35)$$

$$\frac{\partial}{\partial \tau} \ln \left( \frac{\sigma}{(1 + \tau^2)^{1/2}} \rho_R V_\varphi \right) = \lambda \frac{(1 + \tau^2)^{1/2}}{\sigma \rho V_\varphi} \frac{\partial \psi}{\partial \tau}, \quad (36)$$

while  $r$  and  $z$  components of the Generalized Bernoulli Condition (11) will give the following two equations, respectively:

$$\frac{1}{\rho} \frac{\partial p}{\partial \sigma} + \frac{\partial \mathcal{E}_m}{\partial \sigma} + 2(\mathcal{E}_m - \Phi) \frac{\partial}{\partial \sigma} \ln \rho_R = 0, \quad (37)$$

$$\frac{1}{\rho} \frac{\partial p}{\partial \tau} + \frac{\partial \mathcal{E}_m}{\partial \tau} + 2(\mathcal{E}_m - \Phi) \frac{\partial}{\partial \tau} \ln \rho_R = 0, \quad (38)$$

where the total mechanical energy of the system  $\mathcal{E}_m$  [defined by Eq. (24)] is now expressed in similarity variables  $(\sigma, \tau)$ . Hence, in our new framework, the physical system of interest can be analyzed using Eqs. (31,33,35-38).

### 2.4. Variable splitting ansatz

We seek the solution of the system assuming that describing physical variables can be factorized using the similarity variables  $(\sigma, \tau)$  introduced in previous subsection:

$$\begin{aligned} p(\sigma, \tau) &= p_1(\sigma) p_2(\tau), \\ \rho_I(\sigma, \tau) &= \rho_{I1}(\sigma) \rho_{I2}(\tau), \\ \rho_R(\sigma, \tau) &= \rho_{R1}(\sigma) \rho_{R2}(\tau), \\ \lambda(\sigma, \tau) &= \lambda_1(\sigma) \lambda_2(\tau). \end{aligned} \quad (39)$$

The azimuthal velocity can be calculated using the Keplerian rotation velocity  $V_\varphi(\sigma, \tau) = V_{\text{Kep}}$ , where

$$V_{\text{Kep}} = \frac{\sigma_0 \Omega_0}{(1 + \tau^2)^{1/2}} \left( \frac{\sigma}{\sigma_0} \right)^{-1/2}. \quad (40)$$

Here  $\Omega_0$  is the Keplerian angular velocity of the rotation at some characteristic radius  $\sigma_0$  in the disk. Applying this ansatz into Eqs. (31-38), solving them in  $\sigma$ , we find that the balance of all terms give the following solutions in the  $\sigma$  coordinate:

$$\begin{aligned} p_1(\sigma) &= \sigma^{-5/2}, \\ \rho_{I1}(\sigma) &= \sigma^{-1}, \\ \rho_{R1}(\sigma) &= \sigma^{-1/2}, \\ \lambda_1(\sigma) &= \sigma^{-1}. \end{aligned} \quad (41)$$

Having derived the radial profiles of the solution we can now reduce Eqs. (31-38) to the system of ordinary differential equations with respect to  $\tau$ -variable. After some straightforward algebra we obtain:

$$\beta p_2 = (1 + \tau^2)^{3/2} \frac{d\psi}{d\tau} \sigma_0^{3/2} \Omega_0, \quad (42)$$

$$p_2 \rho_2 + \frac{2}{5} (1 + \tau^2)^3 \left( \frac{d\psi}{d\tau} \right)^2 = \frac{2}{5} \frac{\tau^2}{1 + \tau^2} \rho_2^2 \sigma_0^3 \Omega_0^2, \quad (43)$$

where  $\rho_2 \equiv \rho_{I2} \rho_{R2}$ . Introducing notation:

$$W \equiv \frac{1}{\rho_2} \frac{d\psi}{d\tau}$$

we may derive the following algebraic equation:

$$\beta \left[ \beta W(\tau)^2 + \frac{5}{2} \frac{\sigma_0^{3/2} \Omega_0}{(1 + \tau^2)^{3/2}} W(\tau) - \beta \frac{\sigma_0^3 \Omega_0^2 \tau^2}{(1 + \tau^2)^4} \right] = 0. \quad (44)$$

Eq. (44) links the values of the stream-function  $\psi$ ,  $\tau$ -dependent part of density  $\rho_2$  and  $\beta$  parameter and represents the "realizability" condition for all existing solutions within the considered Beltrami flow model of disk-jet structure formation. There are three apparent solutions to this equation:

- (i) The solution with  $\beta = 0$ , corresponding to the background dissipation model ( $T_{ik} = \alpha_0 \mathcal{P}_0$ );
- (ii) Two separate solutions for the dissipative flow ( $\beta \neq 0$ ) with

$$W_{\pm}(\tau) = -\frac{5}{4} \frac{\sigma_0^{3/2}}{(1 + \tau^2)^{3/2}} \frac{\Omega_0}{\beta} \left[ 1 \pm \left( 1 + \frac{16}{25} \frac{\beta^2 \tau^2}{(1 + \tau^2)} \right)^{1/2} \right]. \quad (45)$$

For simplicity of the presentation we may constrain on the small  $\beta$  limit ( $\beta \ll 1$ ). Then the solutions given by (45) can be approximated by the following simplified forms:

$$W_+(\tau) \approx \frac{2}{5} \frac{\tau^2}{(1 + \tau^2)^{5/2}} \beta \sigma_0^{3/2} \Omega_0, \quad (46)$$

$$W_-(\tau) \approx -\frac{5}{2} \frac{1}{(1 + \tau^2)^{3/2}} \frac{\sigma_0^{3/2} \Omega_0}{\beta}. \quad (47)$$

Thus, the solutions of our disk-jet model can be calculated as follows (where  $W(\tau)$  is a general solution of (44)):

$$\rho(\sigma, \tau) = \sigma^{-3/2} \rho_2(\tau), \quad (48)$$

$$p(\sigma, \tau) = \frac{(1 + \tau^2)^{3/2}}{\sigma^{5/2}} \frac{\sigma_0^{3/2} \Omega_0}{\beta} \rho_2(\tau) W(\tau), \quad (49)$$

$$V_r(\sigma, \tau) = -\frac{1 + \tau^2}{\sigma^{1/2}} W(\tau), \quad (50)$$

$$V_z(\sigma, \tau) = -\tau \frac{1 + \tau^2}{\sigma^{1/2}} W(\tau). \quad (51)$$

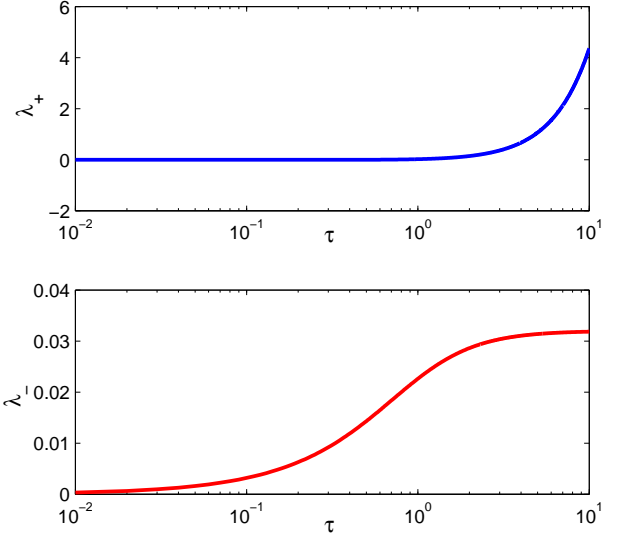


Figure 1: The Beltrami parameters  $\lambda(\tau)$  for the disk (top) and the jet (bottom) solutions are shown vs  $\tau$  for the case when  $\beta = 0.01$ . Notice that Beltrami parameter for the disk solution is negligible for low poloidal angles ( $\tau \ll 1$ ).

Eqs. (49-51) together with radial profiles (41) and appropriate choice of the solution for  $W$  (see Eq. (44)) give the full solution for the disk-jet flow for different types of density profiles  $\rho_2(\tau)$ . Hence, Eqs. (50,51) indicate the character of the solutions corresponding to the different sign of  $W(\tau)$ :

- Radial-vertical accretion flow for  $W_+(\tau) > 0$  corresponding to  $V_r < 0$  and  $V_z < 0$ ;
- Radial-vertical ejection flow for  $W_-(\tau) < 0$  corresponding to  $V_r > 0$  and  $V_z > 0$ ;

Eqs. (31,33,35-38) allow us to calculate dependence of the Beltrami parameter  $\lambda$  on the turbulent viscosity parameter  $\beta$  as follows:

$$\lambda = \left( \frac{dW}{d\tau} + \frac{5\tau W}{1 + \tau^2} \right) \left( (1 + \tau^2) W^2 + \frac{\sigma_0^3 \Omega_0^2}{(1 + \tau^2)^3} \right)^{-1} \sigma_0^{3/2} \Omega_0. \quad (52)$$

Interestingly, both solutions grow with  $\beta$  (see Eqs. (46) and (47)):

$$\lambda_{\pm} = \lambda(W_{\pm}) \propto \beta.$$

Figure 1 shows solutions for the Beltrami parameters  $\lambda_+(\tau)$  and  $\lambda_-(\tau)$  corresponding to the swirling flows that accrete and eject matter, respectively.

Substituting Eqs. (46,47) into (50) and (51) we may derive the velocity field components of the disk flow:

$$V_{rD}(\sigma, \tau) = -\frac{2}{5} \beta \sigma_0 \Omega_0 \frac{\tau^2}{(1 + \tau^2)^{3/2}} \left( \frac{\sigma}{\sigma_0} \right)^{-1/2}, \quad (53)$$

$$V_{zD}(\sigma, \tau) = -\frac{2}{5} \beta \sigma_0 \Omega_0 \frac{\tau^3}{(1 + \tau^2)^{3/2}} \left( \frac{\sigma}{\sigma_0} \right)^{-1/2}, \quad (54)$$

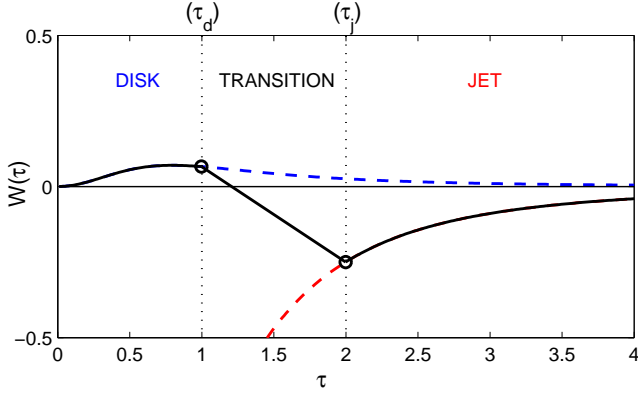


Figure 2:  $W(\tau)$  (solid black line) vs  $\tau$  in three region solution.  $W_+(\tau)$  and  $W_-(\tau)$  are shown by blue and red dashed lines, respectively.  $W(\tau)$  follows  $W_+$  in the disk region and  $W_-$  in the jet region. Transition region in this models starts at  $\tau_d = 1$  and ends at  $\tau_j = 2$ . Within the transition region, where flow is effectively ballistic, disk solution can continuously switch into the jet solution.

and the jet flow:

$$V_{rJ}(\sigma, \tau) = \frac{5}{2} \frac{\sigma_0 \Omega_0}{\beta} \frac{1}{(1 + \tau^2)^{1/2}} \left( \frac{\sigma}{\sigma_0} \right)^{-1/2}, \quad (55)$$

$$V_{zJ}(\sigma, \tau) = \frac{5}{2} \frac{\sigma_0 \Omega_0}{\beta} \frac{\tau}{(1 + \tau^2)^{1/2}} \left( \frac{\sigma}{\sigma_0} \right)^{-1/2}. \quad (56)$$

## 2.5. Disk-jet structure solutions

Analysis present above show that Beltrami flow model for disk-jet structure formation with turbulent viscosity assumption is able to describe classes of solutions corresponding to the accretion disk–ejection jet flow (one flow with the matter and energy). In this model kinematics of the solution can be derived using the realizability parameter  $W(\tau)$  that sets the topology of the solution. To get disk-jet configuration in one solution we need to construct flow that matches the disk solution with  $W_+$  at  $\tau \ll 1$  and jet solution for nearly vertical direction ( $\tau \gg 1$ ). The requirement of the continuity of the velocity field restricts any jumps in  $W(\tau)$ . Hence, to describe the disk-jet solution we use three region model:

- 1.) Disk region for  $\tau < \tau_d$  when  $W(\tau) = W_+(\tau)$ ,
- 2.) Transition region for  $\tau_d < \tau < \tau_j$  when  $\beta = 0$ ,
- 3.) Jet region for  $\tau > \tau_j$  when  $W(\tau) = W_-(\tau)$ ,

where  $\tau_d$  and  $\tau_j$  are the maximal and minimal values of  $\tau$  in the disk and jet regions, respectively. We assume that closer to the central object flow passes through a transition region, where it goes through a ballistic regime, hence, undergoing the dramatic acceleration in vertical ( $z$ ) direction – jet launching. In this region  $\beta = 0$  and “realizability” condition allows any values of  $W(\tau)$ . Hence,  $W_+(\tau_d)$  can switch into  $W_-(\tau_j)$  continuously within the transition region. Figure 2 illustrates the model of  $W(\tau)$  for the proposed three region solution. In this model a

viscous accreting flow in the disk region ( $\tau < \tau_d$ ) goes through inviscid ballistic regime in the transition region ( $\tau_d < \tau < \tau_j$ ) and, finally, into the viscous outflow configuration in the jet region ( $\tau > \tau_j$ ). Hence, the continuous velocity field of this model can be calculated using Eqs. (50), (51) with the three region model of the  $W(\tau)$  function constructed above.

Then we can estimate the accretion speed of the flow in the disk region ( $\tau < \tau_d$ ):

$$V_{\text{acc}} = (V_{rD}^2 + V_{zD}^2)^{1/2} = \frac{2}{5} \frac{\tau^2}{(1 + \tau^2)^{1/2}} \beta V_{\text{Kep}}, \quad (57)$$

and ejection velocity in the jet region ( $\tau > \tau_j$ ):

$$V_{\text{ej}} = (V_{rJ}^2 + V_{zJ}^2)^{1/2} = \frac{5}{2} (1 + \tau^2)^{1/2} \frac{V_{\text{Kep}}}{\beta}. \quad (58)$$

Thus, in the low  $\beta$  limit derived solution corresponds to the locally slowly accreting flow ( $V_{\text{acc}} \ll V_{\text{Kep}}$ ) with the locally fast outflow in the jet region ( $V_{\text{ej}} \gg V_{\text{Kep}}$ ), matching the properties of astrophysical accretion-ejection flows. Notice, that above expressions for local accretion flows in the disk and local outflows in the jet do not depend on the explicit profile of  $\tau$ -dependent part of density. Figure 3 shows the velocity streamlines of the derived disk-jet structure.

To close the system of the disk-jet solutions we need to define angular distribution of the density  $\rho_2(\tau)$  that will be used to obtain different classes of disk-jet structures through Eqs. (48-51). For this purpose we employ the power-law distribution (cf. Shatashvili & Yoshida 2011):

$$\rho_2(\tau) = A_d(\tau + \tau_0)^{m_d} + A_j(\tau + \tau_0)^{m_j}, \quad (59)$$

where parameters  $A_d, m_d$  and  $A_j, m_j$  define the density profile in the disk and jet regions, respectively. The small parameter  $\tau_0 \ll 1$  is used to avoid divergence at the disk center  $\tau = 0$ . Hence, Eqs. (48-51) and (59) describe classes of disk-jet solutions within our self-similar Beltrami flow model. Figure 4 shows the density distribution of the disk-jet structure.

## 2.6. Properties of the disk-jet structure

The purpose of the current paper is to find the analytical solutions constructing a reliable modal for disk-jet structure formation that describe basic properties of hydrodynamic jet outflows from YSOs. Solutions derived in the paper depend on number of parameters. Below we evaluate the possibility of linking these parameters with observational properties of YSOs.

Eqs. (57) and (58) reveal the link of the  $\beta$  parameter with kinematic properties of disk-jet structures:

$$\beta^2 = \frac{V_{\text{acc}}}{V_{\text{ej}}}. \quad (60)$$

The value of  $\beta$  parameter is constrained by the  $\alpha_0$  parameter that describes anomalous viscosity due to background stationary turbulence (see Eqs. (16, 18)):  $\beta < \alpha_0$ . Using a typical value from observational luminosity  $\alpha_0 \sim 0.01$  we can get:

$$V_{\text{ej}} > 10^4 V_{\text{acc}}. \quad (61)$$

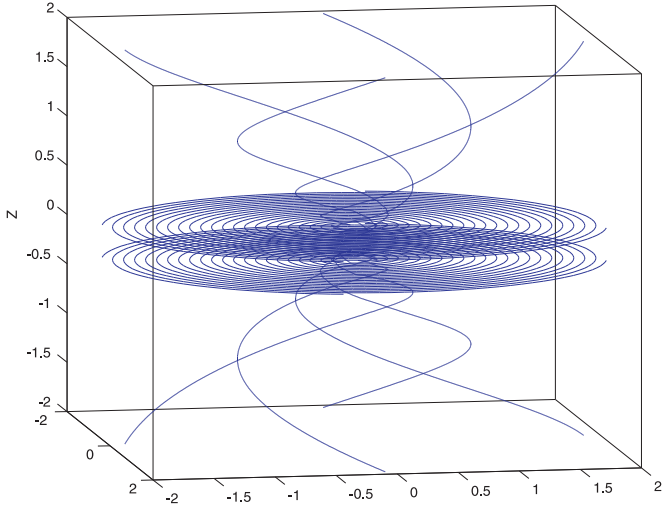


Figure 3: Velocity streamlines of the disk-jet structure illustrating accretion-ejection flow at  $\tau_d = 1$ ,  $\tau_j = 2$ ,  $\tau_0 = 0.01$   $\beta = 0.02$ . Decrease of the  $\beta$  parameter leads to the increase of the ratio between the vertical and radial velocities and, consequently, change of the flow geometry.

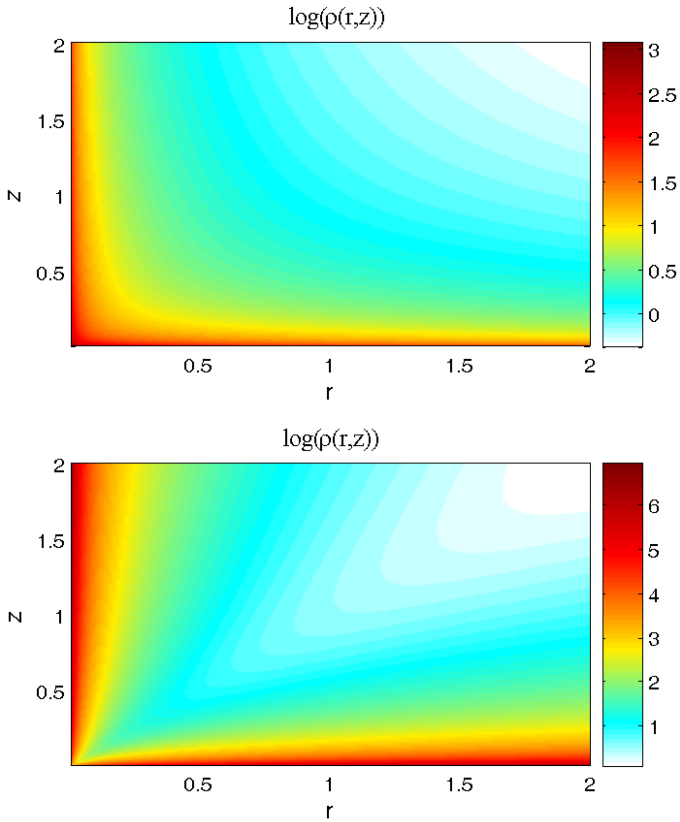


Figure 4: Total density  $\rho(r, z)$  distribution of the disk-jet structure is shown for:  $A_d = 1$ ,  $A_j = 1$ ,  $m_d = -1$ ,  $m_j = 1$  (top) and  $A_d = 3$ ,  $A_j = 3$ ,  $m_d = -3$ ,  $m_j = 3$  (bottom). In all cases  $\tau_0 = 0.01$ . The topology of the density distribution is set by the disk ( $m_d < 0$ ) and the jet ( $m_j > 0$ ) power indices; for  $\rho_2(\tau)$  the power-law distribution (59) was used.

Specific value of the  $\beta$  parameter can be inferred from observations, where both the radial accretion and the vertical ejection velocities near the central object can be observed.

One of the major properties/features of the astrophysical disk-jet flows is their narrow high velocity vertical jets. To illustrate the outflow properties of our solutions the vertical velocity distribution of the jet flow is plotted in Figure 5 (see Eq. (56)). The outflow velocity is maximal at the top edge of transition region, above the disk-plane; beyond this maximum the vertical flow velocity decreases both with vertical and radial distances, similar to the Keplerian profile ( $\propto (\sigma/\sigma_0)^{-1/2}$ ); the outflow launching is at the bottom edge of transition region, just above the disk-surface. Hence, this means that solutions derived within the minimal Beltrami flow model can describe the *formation* of the disk-jet structure (Shatashvili & Yoshida 2011), while the effects of the formed jet acceleration and collimation occur in the vertical outflows farther out from the central object and requires more general dynamical model including the heating/cooling processes.

The standard mechanism of the jet acceleration through purely hydrodynamic mechanism is the Laval nozzle, when adiabatic expansion of the supersonic flow leads to its acceleration. To estimate the feasibility of this mechanism for the derived in this paper disk-jet structure we calculate the local Mach number of the vertical jet flow defined as follows:

$$M_z = \frac{V_{zJ}}{[(\mathcal{P}_0 + p)/\rho]^{1/2}}. \quad (62)$$

Note that pressure variation induced by disk-jet solutions is negative in the jet region ( $p < 0$  when  $W_-(\tau) < 0$ ). Hence, swirling solution in the jet region leads to the decrease of the pressure and corresponding sound speed, thus increasing the local Mach number of the flow. Background pressure can be normalized on the pressure of the self-similar solution at  $\sigma = \sigma_0$  and  $\tau = \tau_j$  (see Eqs. (49, 59)):

$$p_0 \approx \frac{5}{2} \frac{\sigma_0^{1/2} \Omega_0^2}{\beta^2} A_j \tau_j^{m_j}, \quad (63)$$

assuming that  $\tau_0 \ll \tau_j$ . Figure 6 shows local Mach number of the jet outflow for  $\mathcal{P}_0/p_0 = 10^5$ . It seems that the decrease of the vertical outflow velocity coincides with simultaneous decrease of the sound speed, thus, leading to the possible increase of the local Mach number. In the considered extreme limit the flow can reach supersonic velocities in the narrow jet region at  $\tau \gg 1$ . The increase of the background pressure would decrease the local Mach number to the subsonic values. At wider polar angles ( $\tau > 1$ ) vertical flow is subsonic and thus should be decelerating away from the central object (see also Figure 5):

$$V_z(\sigma) \propto \sigma^{-1/2}.$$

Indeed, such wide-angle rotating outflows near the central object together with narrow collimated jets are consistent with ALMA observations of the HH objects (see Arce et al. (2013)).

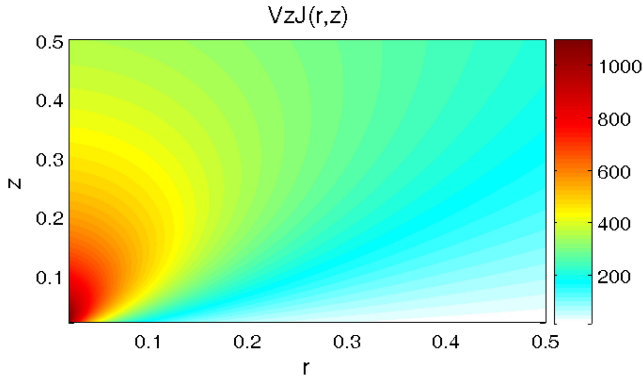


Figure 5: Vertical jet velocity of the jet solution  $V_{z,j}(r, z)/(\sigma_0\Omega_0)$  (see Eq. (56)). Here  $\beta = 0.01$  and  $\sigma_0 = 1$ . Maximal velocity of the outflow is reached near the vertical axis above the disk plane, at the top edge of transition region.

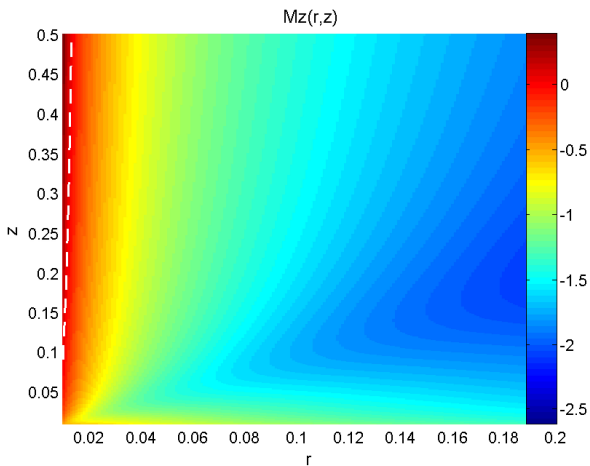


Figure 6: Vertical Mach number of the jet flow  $\log(M_z(r, z))$  when  $A_d = 3$ ,  $A_j = 3$ ,  $m_d = -3$ ,  $m_j = 3$ .  $\tau_0 = 0.01$ ,  $\beta = 0.01$ ,  $\sigma_0 = 1$  and  $\mathcal{P}_0/p_0 = 10^6$ . Vertical dashed line shows area, where the Mach number reveals supersonic flow:  $M_z > 1$ . For density the distribution presented in Figure 4 was used.

Moreover, the outer parabolic shape of the wide-angle outflow near the central object seen in color gradients illustrated in Figure 6 is observed recently for the Class 0 protostellar system by Lee et al. (2018).

In realistic disk-jet systems jet flow streaming away from the central object is likely to undergo cooling (effect not considered in our model) that will further reduce the local sound speed and may render the outflow velocity to become supersonic. In this case farther adiabatic expansion will lead to the jet acceleration – property inherent to the protostellar disk outflows. Thus, solution derived in present study using Generalized Beltrami flow configuration for disk-jet structure can successfully mimic slow radial sub-Keplerian accretion flow in the disk region and fast narrow super-Keplerian outflow in the jet region. The decrease of the  $\beta$  parameter leads to the increase of the ratio between the vertical and radial velocities and, consequently, change of the disk-jet flow geometry.

### 3. Summary

We study the hydrodynamic disk-jet structure formation phenomenon for YSOs based on the analytic Beltrami-Bernoulli model using the extended turbulent viscosity assumption as the main reason of the accretion in the disk. For this purpose we consider the stationary turbulent state powering the accretion process and leading to the collimated jet outflow.

We have employed generalized turbulent viscosity model to describe the effect of turbulent dissipation in both, disk as well as the jet areas of a disk-jet structure. For this purpose we have split the turbulent viscosity tensor into the constant background and varying deviation from the constant profile, leading to the analytic formulation of the viscosity effects in the disk-jet transition area. In this formalism we factorize the local physical parameters of flow into the “ideal fluid” and “reduced” components following Shatashvili & Yoshida 2011 Beltrami-Bernoulli model; this allows to find the self-similar solutions of the disk-jet flow in the field of central gravitating object.

We have formulated the realizability condition for the solutions that reveal the class of disk-jet flow solutions smoothly distributed in three well-defined connected regions of a global structure: a) flow accreting in the radial and vertical direction, b) flow ejecting in the radial and vertical direction; c) flow in the ballistic regime. Hence, constructing the global solution using the disk inflow at low poloidal angles and jet outflow at high poloidal angles, having ballistic transition from one to another, we have derived disk-jet structure with slow accretion and high ejection velocities.

It seems that our disk-jet structure depends on the thermal properties of the disk flow.

Local Mach number of the outflow depends on the background pressure in the jet area. At low pressure, i.e., low temperature values jet outflow may reach supersonic amplitudes close to the central axis of the flow at high poloidal angles. At lower poloidal angles outflow is subsonic, thus showing wide-angle outflow decelerating with radial distance and decrease of the poloidal angle. Considered disk-jet solution describes the formation of the high velocity outflow from slowly accreting Keplerian disk-flow. The further kinematic acceleration and collimation of the jet flow may be due to the effects not considered in the current minimal model. In case of YSOs, our solution shows weaker jets at the later stage of the evolution of protostar, when the temperature of the central object and corresponding disk matter increases.

In our analysis magnetized disk-winds were not invoked – disk was assumed to be not ionized (hence, magnetic fields can not affect the flow structure). We believe, that additional effects of magnetic fields (self-consistently generated or advected, or their combination) will make the solution of the problem only richer; the consequent problems of jet acceleration and heating could be also discussed then. Due to Hall effect the generalized magneto-Bernoulli mechanism (Mahajan et al. 2002, 2006) may effectively accelerate the jet-flow. In a weakly ionized plasma the Hall effect is magnified by the ratio of the neutral and electron densities; the ambipolar diffusion effect also yields



a higher-order perturbation (Krishan & Yoshida 2006). The disk-jet connection point may differ depending on the plasma condition near the central object: e.g. in AGN, the plasma is fully ionized but rather collisional (we also need a relativistic equation of state with possible presence of pairs). Also the details of dissipation mechanism may play the additional role. Such issues will be discussed in our future works.

Analytic solutions for disk-jet structure derived in the present paper can be used to analyze the properties of hydrodynamic jets from YSOs, and link their topological properties to the local physical conditions at the jet launching areas.

Our derived Disk-jet solutions describe the astrophysical disk-jet structures with low ionization, where the main energy source of the outflow should come from non-magnetic processes. These should include hydrodynamic jets from protostellar accretion disks and young stellar objects in general. Our analytic model links the accretion and ejection rates of the disk-jet flow, thus allowing to propose the specific predictions for observed structures.

## Acknowledgments

Authors express special thanks to Prof. Zensho Yoshida for his valuable discussions. E.A., B.M., M.G., V.L. and I.J. acknowledge support from the TSU Student Research Council and the TSU Faculty of Exact and Natural Sciences Students Grant; M.G.-s and I.J.-s work was partially supported by World Federation Of Scientists National Scholarship Programme Geneva, 2018; NLS-s, M.G.-s and I.J.-s research was partially supported by Shota Rustaveli Georgian National Foundation Grant Project No. FR17-391.

## References

Arce, H. G., Mardones, D., Corder, S. A., Garay, G., Noriega-Crespo, A., Raga, A. C., 2013 *ApJ*, 774, 39  
 Anderson, J. M., Li, Z. Y., Krasnopolsky, R. and Blandford, R. D., 2005 *ApJ*, 630, 945  
 Bally, J., 2016 *Ann. Rev. Astron. Astrophys.*, 54, 491  
 Begelman, M. C., Blandford, R. D. and Rees, M. J., 1984 *Rev. Mod. Phys.* 56, 255  
 Begelman, M. C., 1993 "Conference summary", in *Astrophysical Jets*, ed. D. Burgarella et al (Cambridge: Cambridge Univ. Press), 1993, pp. 305-315.  
 Begelman, M. C., 1998 *ApJ*, 493, 291  
 Belan M., Massaglia S., Tordella D., Mirzaei M., and de Ponte S., 2013, *A&A*, 554, A99  
 Bisnovaty-Kogan G. S. and Lovelace, R.V.E., 2007, *ApJ* 667(2), L167-L169  
 Blandford, R. D. and Rees, M. J., 1974 *MNRAS*, 169, 395  
 Blandford, R. D. and Znajek, R. L., 1977 *MNRAS*, 179, 433  
 Blandford, R. D. and Payne, D. G., 1982 *MNRAS*, 199, 883  
 Blandford, R. D., 1994 *ApJS*, 90, 515  
 Bjerkeli, P., van der Wiel, M. H. D., Harsono, D., Ramsey, J. P., Jorgensen, J. K., 2016, *Nature*, 540, 406  
 Celotti, A. and Blandford, R. D., "Black Holes in Binaries and Galactic Nuclei: Diagnostics, Demography and Formation", in *ESO Astrophysics Symposia* ed. L. Kaper *et al.* (Berlin, Heidelberg: Springer-Verlag), 2001, 206.  
 Clarke, C. J., and Alexander, R. D., 2016 *MNRAS*, 460, 3044  
 Ferreira, J., 1997, *A&A* 319, 340  
 Ferreira, J., Dougados, C. and Cabrit, S., 2006 *A&A* 453, 785 (2006); Ferreira, J., Dougados, C. and Whelan, E., *Jets from Young Stars I: Models and Constraints in Lecture Notes in Physics* ed. Ferreira, J. et al. (Berlin, Heidelberg: Springer-Verlag) 2007, 723, 181.

Hartigan P., Frank A., Foster J. M., Wilde B. H., Douglas M., Rosen P. A., Coker R. F., Blue B. E., and Hansen J. F., 2011, *ApJ*, 736, 29  
 Hernandez, X., Rendon, P. L., Rodriguez-Mota, R. G., and Capella A., 2014 *Rev. Mex. Astr. Astrophys.* 50, 23.  
 Ioannidis, G., Froebrich, D., 2012, *MNRAS*, 421, 3257  
 Jhan, K.-S., Lee, C.-F., 2016, *ApJ*, 816, 1  
 Krasnopolsky, R., Li, Z. Y. and Blandford, R. D., 1999 *ApJ*, 526, 631  
 Krishan V., Yoshida Z., 2006 *Phys. Plasmas*, 13, 092303  
 Kudoh, T. and Shibata, K., 1987 *ApJ*, 474, 362  
 Kuwabara, T., Shibata, K., Kudoh, T. and Matsumoto, R., 2005 *ApJ*, 621, 921  
 Lee, C.-F., Ho, P. T., Li, Z.-Y., Hirano, N., Zhang, Q., Hsien, S., 2017, *Nature Astr.*, 1, 0152  
 Lee, C.-F., Li, Z.-Y., Codella, C., Ho, P. T. P., Podio, L., Hirano, N., Shang, H., Turner, N. J., Zhang, Q., 2018 *ApJ*, 856, 14  
 Livio, M. "The Formation Of Astrophysical Jets", in *Accretion Phenomena and Related Outflows*; IAU Colloquium 163 ed. D. T. Wickramasinghe et al (San Francisco: ASP) ASP Conference Series 1997, 121, 845.  
 Lizano, S., Heiles, C., Rodriguez, L. F., Koo, B.-C., Shu, F. H., Hasegawa, T., Hayashi, S., Mirabel, I. F., 1988 *ApJ*, 328, 763  
 Lovelace, R.V.E., Romanova, M.M. and Newman, W.I., 1994, *ApJ*, 437, 136  
 Lubow, S.H., Papaloizou, J.C.B. and Pringle, J.E., 1994, *MNRAS* 267, 235  
 Mahajan S. M., Nikol'skaya K. I., Shatashvili N. L., Yoshida Z., 2002 *ApJ*, 576, L161  
 Mahajan S. M., Shatashvili N. L., Mikeladze S. V., Sigua K. I., 2006 *Phys. Plasmas*, 13, 062902  
 Moss, V. A., McClure-Griffiths, N. M., Murphy, T., Pisano, D. J., Kummerfeld, J. K., Curran, J. R., 2013, *ApJS*, 209, 12  
 Plunkett, A. L., Arce, H. G., Mardones, D., van Dokkum, P., Dunham, M. M., Fernandez-Lopez, M., Gallardo, J., Corder, S. A., 2015, *Nature*, 527, 70  
 Podio, L., Codella, C., Gueth, F., Cabrit, S., Maury, A., Tabone, B., Lefevre, C., Anderl, S., Andre, P., Belloche, A., Bontemps, S., Hennebelle, P., Lefloch, B., Maret, S., Testi, L., 2016, *A&A*, 593, L4  
 Reiter, M., Kiminki, M. M., Smith, N., Bally, J., 2017, *MNRAS*, 467, 4441  
 Ruden, S. P., Glassgold, A., and Shu, F., 1990 *ApJ*, 361, 546  
 Scott, H. A. and Lovelace, R. V. E., 1987, *Ap. & SS*, 129, 361  
 Shu, F., Ruden, S. P., Lada, C. J., Lizano, S., 1991 *ApJ*, 370, L31  
 Squire, H. B., 1951 *Quart. J. Mech. Appl. Math.*, 4, 321  
 Shakura, N. I., Sunyaev, R. A., 1973, *A&A*, 24, 337  
 Shatashvili, N.L. and Yoshida, Z., 2011, *AIPCP*, 1445, 34-53  
 Smith, M. D., Davis, C. J., Rowles, J. H., Knight, M., 2014, *MNRAS*, 443, 2612  
 Tordella, D., Belan, M., Massaglia, S., De Ponte, S., Mignone, A., Bodenschatz, E., Ferrari, A., 2011, *New J. Phys.*, 13, 043011  
 Yoshida, Z., Shatashvili N. L., 2012, *arXiv:1210.3558*  
 Zanni, C., Ferrari, A., Rosner, R., Bodo, G. and Massaglia, S., 2007 *A&A*, 469, 811  
 Zhang, M., Wang, H., Hennings, T., 2014, *AJ*, 148, 26